Static-FE Harmonic Analysis of PM Slip Couplers

Dillan K. Ockhuis, *Student Member, IEEE* and Maarten J. Kamper, *Senior Member, IEEE*
Department of Electrical and Electronic Engineering, Stellenbosch University, South-Africa
Email: d.ockhuis09@gmail.com; kamper@sun.ac.za

***Abstract*—In this paper, a 2-D static finite element (S-FE) analysis method of a slip-magnetic coupling is proposed. The FE analysis method uses the frozen permeability technique, which allows the user to accurately determine the relevant model parameters by including the effects of saturation and cross-coupling. Moreover, the proposed analysis method accurately predicts the zero-sequence (3^{rd} harmonic) and higher-order harmonic induced voltages and currents which are present in magnetic couplings. It is found that the zero-sequence and higher-order harmonic currents contribute to the net-torque of the magnetic coupling and their effects are more prevalent at low loads. The method is verified by means of comparing its results to those obtained from a commercial transient FE (T-FE) package. The S-FE method solutions are verified over a wide slip range, and are shown to be significantly less computationally time intensive compared to the T-FE package.**

***Index Terms*—Magnetic coupling, zero-sequence analysis, harmonics, finite-element analysis, permanent magnet, radial flux.**

I. Introduction

Magnetic couplings (MCs) are of particular interest in industrial applications because they allow torque to be transferred between two systems without mechanical contact. This has numerous advantages including a reduction in noise, vibration, protection and friction between the coupled systems. However, modelling and predicting the torque performance of MCs is challenging as it requires an accurate solution of a complex 3-D magnetic field problem.

In literature, both numerical and analytical methods are used to solve the magnetic field distribution problem. Numerical methods which use 2-D and 3-D finite element (FE) analysis [1]–[5] gives accurate results, however, it is argued that they are too computationally-time intensive. In contrast, it is argued that analytical methods require far less computational time because they are based on underlying assumptions which greatly simplifies the problem. The most widely used analytical methods involve solving the torque and force between two magnets based on the magnets' geometry [6]–[9], or by employing magnetic equivalent circuits [10]–[14] or by dividing the geometry of the MC into domains (PM, air-gap, iron, etc) and then solving the magnetic field problem in each of the subdomains [15]–[21]. These analytical methods, however, are restricted to slotless MCs and aren't easily applicable to MCs with slotted configurations due to the inherent complexity of slotted geometries. The paper by [22] proposes an analytical method to predict the magnetic field in axial-flux MCs with a slotted conductor topology, however, the inherent complexity of the slotted conductor design resulted in inaccuracies in predicting torque when compared to 2-D and 3-D FE analysis methods.

A study conducted in [23] found that by replacing the slotless MC topology with a toothed configuration, similar to those used in conventional electrical machines, results in a significant reduction in the PM mass required to generate a comparable torque response over the feasible slip range. The toothed-MC topologies considered in [23] are referred to as slip-permanent magnetic couplers (S-PMC).

S-PMCs consists of two rotors separated by an air-gap. One rotor is equipped with PMs and the other consists of a toothed-stator which is equipped with individually short-circuited coils. In [24], a 2-D-FE analysis method is proposed to model and predict the torque performance of S-PMCs, however, the method of [24] has a few drawbacks. It does not include the effects of saturation by neglecting the effects of cross-coupling. Additionally, the method neglects the harmonics due to the PM rotor by assuming purely sinusoidal coil currents which is shown to be inaccurate for certain slot configurations. Furthermore, it is unclear as to what influence these higher-order harmonics has on the current and torque of the S-PMC.

The contribution of this paper is to propose a 2-D Static-FE (S-FE) methodology to quickly and accurately model and analyse S-PMCs. The proposed method allows the user to determine the zero-sequence and higher-order harmonic current components which are present in these types of S-PMCs, something which has hitherto been ignored. By incorporating the higher order harmonics, an accurate solution of the coil currents and hence the S-PMC torque can be obtained. Additionally, the method incorporates the effects of saturation and cross-coupling by using the frozen permeability method [25]–[29]. Furthermore, this method provides the user with a method to quickly and accurately determine the model and performance parameters of S-PMCs for design optimization purposes. The proposed methodology is verified by comparing its results to the results of a commercial transient-FE package.

II. Modelling

In this section an analytic model of the S-PMC in Fig. 1a is derived. The considered S-PMC consists of 28 magnet poles, 30 slots and 30 individually short-circuited, non-overlap coils. An example of one such short-circuited coil is shown in Fig. 1b. In [24], it is shown that the 30 short-circuited coils of the S-PMC can be divided into 10 balanced three-phase sets. Moreover, due to symmetry, 15 adjacent coils can further be divided into 5 three-phase coil sets to form a complete winding. Fig. 1c shows a phase-vector diagram of a generalized n-phase S-PMC. If we first consider only one three-phase set, then from the *dq0* voltage equations of a

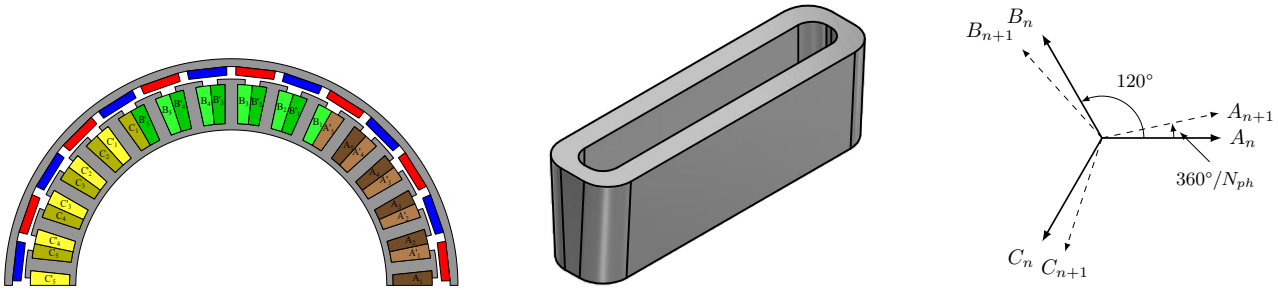

(a) (b) (c)

Fig. 1: (a) FE model of a multi-phase slip coupler, (b) example of an individual short-circuited coil, e.g. $A_1 - A_1^{'}$, and (c) vector diagram for the n^{th} three phase coil set.

three-phase winding PM synchronous machine we have

$$\begin{aligned} v_d &= R_s i_d + \frac{d\lambda_d}{dt} - \lambda_q \omega_e \\ v_q &= R_s i_q + \frac{d\lambda_q}{dt} + \lambda_d \omega_e \\ v_o &= R_s i_o + \frac{d\lambda_o}{dt}. \end{aligned} \tag{1}$$

where the flux linkages are functions of i_q, i_d, i_o, α, and λ_m. The electrical angular position of the rotor is given by α, and λ_m is the PM stator flux linkage.

If we consider average inductances with rotor position and average (steady-state) I_d and I_q currents (that we want to solve) and thus average λ_d and λ_q flux linkages, then for the considered S-PMC with its short-circuited stator windings (1) simplifies to

$$\begin{aligned} 0 &= R_{sn} I_{dn} - \lambda_{qn} \omega_e \qquad \text{(a)} \\ 0 &= R_{sn} I_{qn} + \lambda_{dn} \omega_e \qquad \text{(b)} \\ 0 &= R_{sn} i_{on} + \frac{d\lambda_{on}}{dt}, \qquad \text{(c)} \end{aligned} \tag{2}$$

where the subscript n denotes the set number of a particular three-phase coil set where n = 1, 2, ..., 5. Each of the individually short-circuited coils have identical coil currents such that I_{d1} = I_{d2} = ... = I_{d5} = I_d and I_{q1} = I_{q2} = ... = I_{q5} = I_q. Consequently, the total d-axis flux linkage for the first coil set, n = 1, can be written as

$$\begin{aligned} \lambda_{d1} =& [L_{d(1,1)} + L_{d(1,2)} + ... + L_{d(1,5)}] I_d \\ &+ [L_{dq(1,1)} + L_{dq(1,2)} + ... + L_{dq(1,5)}] I_q \\ &+ \lambda_{dm(1)} \\ =& L_{d1} I_d + M_{dq1} I_q + \lambda_{dm1}. \end{aligned} \tag{3}$$

Similarly, the total q-axis and the zero-axis flux linkages for the first coil set n = 1 can be written as

$$\begin{aligned} \lambda_{q1} =& [L_{q(1,1)} + L_{q(1,2)} + ... + L_{q(1,5)}] I_q \\ &+ [L_{qd(1,1)} + L_{qd(1,2)} + ... + L_{qd(1,5)}] I_d \\ &+ \lambda_{qm(1)} \\ =& L_{q1} I_q + M_{qd1} I_d + \lambda_{qm1}, \end{aligned} \tag{4}$$

and

$$\begin{aligned} \lambda_{o1} =& [L_{o(1,1)} + L_{o(1,2)} + ... + L_{o(1,5)}] i_o + \lambda_{om(1)} \\ =& L_{o1} i_o + \lambda_{om1}. \end{aligned} \tag{5}$$

The flux linkages of equation (2) can now be rewritten in general for any particular coil set as

$$\begin{aligned} \lambda_d &= L_d I_d + M_{dq} I_q + \lambda_{dm} \qquad \text{(a)} \\ \lambda_q &= L_q I_q + M_{qd} I_d + \lambda_{qm} \qquad \text{(b)} \\ \lambda_o &= L_o i_o + \lambda_{om}, \qquad \text{(c)} \end{aligned} \tag{6}$$

where L_d, L_q and L_o are the respective total $dq0$-axis self-inductances, and M_{dq} = M_{qd} are the respective total dq-axis cross-coupling mutual-inductances. It should be noted that 3-D effects such as the end-winding resistance and inductance are calculated and accounted for as per [30] and are included in R_{sn} and L_{dq0} in (2) and (6) respectively.

If we substitute λ_q and λ_d into (2a) and (2b) respectively, and re-write the resulting equations in matrix form, we obtain

$$\mathbf{I}_{dq} = \mathbf{Z}_{dq}^{-1} \mathbf{E}_{dq}, \tag{7}$$

where

$$\mathbf{E}_{dq} = \begin{bmatrix} \omega_e \lambda_{qm} & -\omega_e \lambda_{dm} \end{bmatrix}^T, \tag{8}$$

$$\mathbf{I}_{dq} = \begin{bmatrix} I_d & I_q \end{bmatrix}^T \tag{9}$$

and

$$\mathbf{Z}_{dq} = \begin{bmatrix} (R_s - \omega_e M_{qd}) & -\omega_e L_q \\ \omega_e L_d & (R_s + \omega_e M_{dq}) \end{bmatrix}. \tag{10}$$

III. Zero-Sequence Analysis

We are particularly interested in the alternating zero-sequence (3^{rd} harmonic) current component of (1). By considering the zero-sequence components of (2c) and (6c),

$$\begin{aligned} \frac{d\lambda_o}{dt} &= L_o \frac{di_o}{dt} + \frac{\partial \lambda_{om}}{\partial \alpha} \frac{d\alpha}{dt} \\ &= L_o \frac{di_o}{dt} + k_o \omega_e \qquad \left[k_o = \frac{\partial \lambda_{om}}{\partial \alpha} \right], \end{aligned} \tag{11}$$

we see thus that an alternating voltage is induced in the zero-sequence winding by the varying zero-sequence PM flux linkage. By assuming only a 3^{rd} zero-sequence harmonic, which is a valid approximation as the higher-order zero-sequence harmonics are very small, then the 3^{rd} harmonic

zero-sequence harmonic flux linkage in phase a and in the zero-sequence circuit due to the PM can be expressed by the general form as

$$\lambda_{am(3)} = \lambda_{om(3)} = -\lambda_{m(3)} \cos(3\alpha + \phi_{(3)}). \tag{12}$$

The minus sign in (12) is normally the case for the 3^{rd} harmonic. The peak value of the flux linkage of (12) is determined by the Fourier transform method described in Section IV. Using (12), the 3^{rd} harmonic induced voltage in the zero-axis circuit is given from (11) by

$$e_{o(3)} = k_{o(3)}\omega_e = 3\omega_e \lambda_{m(3)} \sin(3\alpha), \tag{13}$$

where $\alpha = \omega_e t$. From (2c), (11) and (13) it follows that

$$3\omega_e \lambda_{m(3)} \sin(3\omega_e t) = R_s i_{o(3)} + L_{o(3)} \frac{di_{o(3)}}{dt}. \tag{14}$$

From (13), the peak zero-sequence harmonic voltage is given by

$$E_{o(3)} = 3\omega_e \lambda_{m(3)}, \tag{15}$$

and hence the peak zero-sequence harmonic current, according to (14), by

$$I_{o(3)} = \frac{E_{o(3)}}{\sqrt{R_s^2 + X_{o(3)}^2}}, \tag{16}$$

where $X_{o(3)} = 3\omega_e L_{o(3)}$. The latter inductance $L_{o(3)}$ can be determined from the frozen permeability method. The zero-sequence current can be expressed from (14) and (16) as

$$i_{o(3)}(t) = I_{o(3)} \sin(3\omega_e t - \theta_{o(3)}), \tag{17}$$

where $\theta_{o(3)}$ is the zero-sequence power factor angle given by

$$\theta_{o(3)} = \tan^{-1}\left(\frac{X_{o(3)}}{R_s}\right). \tag{18}$$

IV. FEA Computation of Coil Currents

It should be noted that the coil currents, and hence the performance, of the slip coupler isn't known for a given slip value. Consequently, in this section, a solution method is proposed to verify the analytical derivations outlined in the previous sections whereby the $dq0$-axis inductances and coil currents of (6) are determined. To achieve this, a S-FE, frozen permeability method (FPM) is used.

In the FPM, the iron magnetic permeabilities of each S-FE mesh element is fixed or "frozen" (for a given rotor position) after each non-linear S-FE solution to preserve the information regarding the saturation of the machine at the specified load condition and rotor position. By freezing the iron magnetic permeabilities, the non-linear problem turns into a linear problem and additional (fast) linear S-FE solutions can be used to determine the individual flux linkage components of $\boldsymbol{\lambda}_{dq0}$ as expressed in (6).

A. Harmonic Components

Fig. 2 shows the theoretical PM-rotor MMF harmonics for a 28-pole, 30-slot S-PMC with a magnet pitch of σ_m = 100%. From Fig. 2, it can be seen that the higher-order rotor MMF harmonics aren't insignificant and will induce voltages and currents in the short-circuited coils of the S-PMC at various harmonic frequencies. These higher-order harmonics will alter the shape of the coil currents and cause them to become non-sinusoidal.

To solve the harmonic currents of (7), the PM flux linkages of (8) and the impedances of (10) must be determined. To do this, the phase currents and flux linkages are expressed in terms of Fourier components as

$$s_{abc}(\alpha) = \begin{cases} s_a(\alpha) = \sum_{k=1}^{m} A_k \cos(k\alpha + \phi_k) \\ s_b(\alpha) = \sum_{k=1}^{m} A_k \cos(k\alpha + \phi_k - \frac{2\pi}{3}) \\ s_c(\alpha) = \sum_{k=1}^{m} A_k \cos(k\alpha + \phi_k + \frac{2\pi}{3}) \end{cases} \tag{19}$$

where $s_{abc}(\alpha)$ are the phase-domain FE variables, k represents the harmonic order, A_k is the amplitude of the k^{th} harmonic component, ϕ_k denotes the phase shift of a given signal and m denotes the highest-order harmonic component considered within a phase-domain signal. The Park transform can then be utilized on the respective harmonic components of $s_{abc}(\alpha)$ to obtain the respective dq-axis harmonic components in the harmonic rotor reference frames as

$$\begin{aligned} S_{d(k)}(\alpha) &= \frac{2}{3} A_k \cos(\phi_k) \\ S_{q(k)}(\alpha) &= -\frac{2}{3} A_k \sin(\phi_k) \end{aligned} \tag{20}$$

and the inverse as

$$\begin{bmatrix} s_{a(k)}(\alpha) \\ s_{b(k)}(\alpha) \\ s_{c(k)}(\alpha) \end{bmatrix} = \mathbf{K}_{\mathrm{p}}^{-1}(k\alpha) \begin{bmatrix} S_{d(k)} \\ S_{q(k)} \end{bmatrix}, \tag{21}$$

where $\mathbf{K}_{\mathrm{p}}^{-1}(k\alpha)$ is the inverse Park transformation matrix.

B. PM-Flux Linkages

To solve for the dq PM flux linkages of (8), 2ν non-linear S-FE solutions are run at 2ν rotor positions for a given current $i_{abc}(\alpha)$, where the rotor positions are equally spaced across a magnet pole pitch and where ν is the number of harmonic

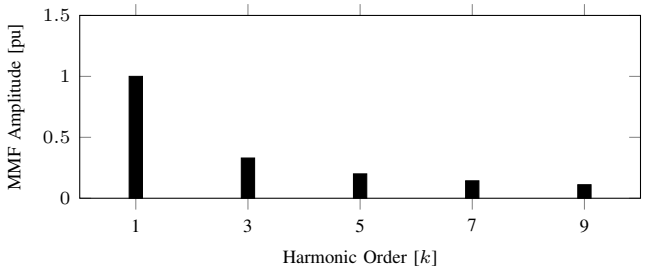

Fig. 2: Per-unit PM-rotor MMF harmonics for a 28-pole, 30-slot S-PMC with a magnet pitch of σ_m = 100% (per unit values are calculated with the working harmonic as the base value, where the working harmonic is $n_r = 1 \times 7$).

components being solved [e.g. if only the 1^{st}, 3^{rd} and 5^{th} harmonics of Fig. 2 are considered, then ν = 3]. The PM flux linkage $\lambda_{abcm}(\alpha)$ values at the 2ν positions are then obtained by the FPM with $i_{abc}(\alpha)$ = 0 used in the linear S-FE solutions. With $\lambda_{abcm}(\alpha)$ known, the Fourier constants A_k and ϕ_k are determined using (19) and from that, the harmonic flux linkages $\lambda_{dm(k)}$ and $\lambda_{qm(k)}$ are determined using (20). Note that $\lambda_{m(3)}$ of (13) and (14) is already obtained from (19).

C. Inductances

The FPM is used to determine the $dq0$-inductances by setting the excitation due to the PMs to zero and executing linear FE solutions where the machine is excited with only $I_{d(k)}$, $I_{q(k)}$, or $i_{o(3)}$ currents respectively, where k represents the harmonic order of a particular current input. The total respective $dq0$ inductances for each harmonic order can then be determined by

$$\begin{aligned} L_{d(k)} &= \frac{\lambda_{dd(k)}}{I_{d(k)}}\bigg|_{I_q=i_o=0} & M_{qd(k)} &= \frac{\lambda_{qd(k)}}{I_{d(k)}}\bigg|_{I_q=i_o=0} \\ L_{q(k)} &= \frac{\lambda_{qq(k)}}{I_{q(k)}}\bigg|_{I_d=i_o=0} & M_{dq(k)} &= \frac{\lambda_{dq(k)}}{I_{q(k)}}\bigg|_{I_d=i_o=0} \\ L_{o(3)} &= \frac{\lambda_{oo(3)}}{i_{o(3)}}\bigg|_{I_d=I_q=0} \end{aligned} \tag{22}$$

where $\lambda_{dd(k)}$, $\lambda_{qq(k)}$, and $\lambda_{oo(3)}$ are the respective flux linkages resulting from linear FE solutions where only k^{th}-order d-axis currents or q-axis currents or zero-axis currents respectively are used to excite the machine. Moreover, $\lambda_{qd(k)}$ is the q-axis cross-coupling flux linkage due to the k^{th}-order d-axis current. Similarly, $\lambda_{dq(k)}$ is the d-axis cross-coupling flux linkage due to the k^{th}-order q-axis current.

D. Solving Coil Currents

Since the coil currents of the slip coupler aren't known for a given slip value, an iterative technique is required to solve the coil currents at a specific load condition. The iterative technique is outlined as follows:

1) The $dq0$ PM flux linkages are determined as outlined in Section IV-B. An initial set of $dq0$ inductances are then obtained by solving linear FE solutions with k^{th}-order current inputs as outlined in (22).
2) The dq voltage matrix $\mathbf{E}_{dq}$ of (8) and the dq impedance matrix $\mathbf{Z}_{dq}$ of (10) can now respectively be determined for each harmonic component, along with the zero-sequence reactance $X_{o(3)} = 3\omega_e L_{o(3)}$. Equation (7) can now be solved separately for each harmonic component in terms of the current matrix $\mathbf{I}_{dq(k)}$ of (9) and an updated set of dq harmonic currents are obtained.
3) With $\lambda_{m(3)}$ known from the first step, the peak value of the zero-sequence voltage $E_{o(3)}$ is determined from (15) and the peak value of the zero-sequence current is determined from (16). The zero-sequence power factor angle is determined from (18).
4) The updated $dq0$-harmonic currents are separately transformed into their respective abc-harmonic currents using (21) and are compared to the previous iteration's results. Steps 1) to 4) are iterated until each harmonic current component converges.

Fig. 3 shows the results of the RMS current $I_{rms(1)}$ of the fundamental harmonic component versus a convergence iterator Q for various slip (load) conditions. Fig. 3 reveals that the proposed S-FE method requires at least Q = 4 iterations for the currents to converge for the considered slip values which indicates the proposed method's speed and effectiveness.

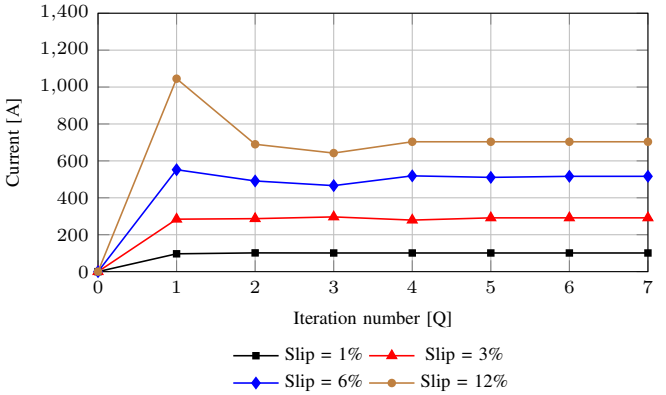

Fig. 3: RMS current of the fundamental (k = 1) harmonic component versus iteration number for slip values: s = 1%, 3%, 6% and 12%.

V. Developed Torque

It must be noted from the steady-state modelling of (2) that the dq-currents and flux linkages are DC quantities, while the zero-sequence current and flux linkages are AC quantities. The instantaneous power from the circuit equations of (2) is given for a three-phase winding by

$$p_{dq0} = \frac{3}{2}[\lambda_d \omega_e I_q - \lambda_q \omega_e I_d + 2k_{o(3)}\omega_e i_{o(3)}]. \tag{23}$$

Using (6) and (13), (23) becomes

$$\begin{aligned} p_{dq0} &= \frac{3}{2}\omega_e[\lambda_{dm} I_q - \lambda_{qm} I_d + (L_d - L_q) I_d I_q \\ &\quad + M_{dq}(I_q^2 - I_d^2) + 6\lambda_{m(3)} \sin(3\alpha) i_{o(3)}] \\ &= s\omega_s[T_{pm} + T_r + T_m + \tau_{o(3)}] \\ &= s\omega_s[T_d + \tau_{o(3)}], \end{aligned} \tag{24}$$

where $s\omega_s$ is the slip speed and s the slip defined by

$$s = \frac{\omega_t - \omega_s}{\omega_s}, \tag{25}$$

and where ω_s is the synchronous output speed and ω_t the input speed of the coupler which is defined as

$$\omega_t = (1 + s)\omega_s. \tag{26}$$

Hence, from the above, the slip-coupler torque can then be described by

$$\begin{aligned} T_{pm} &= \frac{3}{4}p[\lambda_{dm} I_q - \lambda_{qm} I_d] && (a) \\ T_r &= \frac{3}{4}p[L_d - L_q] I_d I_q && (b) \\ T_m &= \frac{3}{4}p M_{dq}[I_q^2 - I_d^2] && (c) \\ \tau_{o(3)} &= \frac{9}{2}p\lambda_{m(3)} \sin(3\alpha) i_{o(3)}, && (d) \end{aligned} \tag{27}$$

where T_{pm} is the rotor PM-flux torque and T_r, T_m, $\tau_{o(3)}$ are the respective reluctance, cross-magnetization and zero-sequence torque components. If we focus for a moment on the zero-sequence torque of (27d). Replacing the zero-sequence current of (27d) by (17) we get

$$\begin{aligned}\tau_{o(3)} &= \frac{9}{2}p\lambda_{m(3)}I_{o(3)}\sin(3\alpha)\sin(3\alpha-\theta_{o(3)}) \\ &= \frac{9}{4}p\lambda_{m(3)}I_{o(3)}[\cos(\theta_{o(3)})-\cos(6\alpha-\theta_{o(3)})] \\ &= \frac{9}{4}p\lambda_{m(3)}I_{o(3)}[1-\cos(6\alpha)] \quad [\text{assuming} \quad \theta_{o(3)}\approx 0] \\ &= T_{o(3)}-\tau_{a(3)}.\end{aligned} \tag{28}$$

This result shows that the zero-sequence induced voltage and current in the S-PMC generates a DC- and an alternating component of torque. If the torque equations of (27a) - (27c) are calculated for each harmonic component k, the total generated torque of the S-PMC is calculated by

$$T_{net} = N\left[T_{o(3)} + \sum_{k=1}^{m} T_{d(k)}\right] \tag{29}$$

where N = 5 is the number of balanced three-phase sets. The total conduction losses can then be calculated by

$$P_{cu} = s\omega_s T_{net} \tag{30}$$

VI. Results

In this section, the performance and the computed parameter results using the solution method proposed in Section IV are given for the 28-pole, 30-slot S-PMC of Fig. 1. The dimensions and parameters of the considered S-PMC are given in Table I.

In the analysis, the highest-order harmonic selected was m = 5, then ν = 3 according to Fig. 2 and solutions at six rotor positions are required to determine the harmonic components. The proposed method's results are compared and validated with the commercial transient-FE package *JMAG Designer*.

A. Flux Linkage

Fig. 4 shows the S-FE-determined PM-flux linkages at rated slip. From this, it is clear that there is a zero-sequence PM-flux linkage component present. Additionally, there is a small contribution of the fundamental q-axis PM-flux linkage $\lambda_{qm(1)}$, however, the fundamental d-axis PM-flux linkage $\lambda_{dm(1)}$ is the dominant contributor to the PM-flux linkage.

TABLE I
DIMENSION AND PARAMETER VALUES OF THE SLIP COUPLER.

Dimension	Value	Parameter	Value
Outer diameter	173.5 mm	Rated output speed	600 rpm
Inner diameter	118.9 mm	Rated slip	3%
Wound rotor yoke	2.99 mm	Number of poles	28
Tooth height	15 mm	Number of slots	30
Tooth width	4.86 mm	Magnet type	NdFeB (N48H)
Coil height	14.8 mm	Coil resistance	60 uΩ
Magnet height	3.27 mm	Current density	3.71 A/mm^2
Magnet pitch	81%	Rated power	2.5 kW
Air gap	1.2 mm	Rated torque	40 Nm
Axial length	54.74 mm	Rated frequency	4.3 Hz

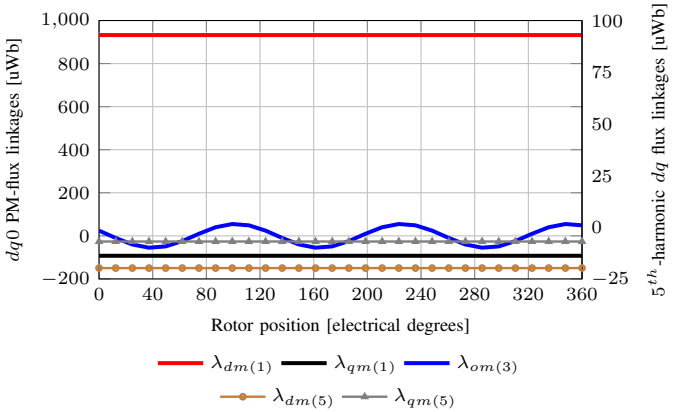

Fig. 4: Static-FE-determined PM-flux linkage component results obtained from a linear FE solution where the $I_{dq0(k)}$ = 0. The fundamental and zero-sequence harmonic flux linkages are on the primary y-axis and the 5^{th}-harmonic dq flux linkages are on the secondary y-axis.

Also shown are the 5^{th} harmonic dq PM-flux linkages. It can be seen that the 5^{th} harmonic dq PM-flux linkages are relatively small and of comparable magnitude.

B. Performance Results

Table II provides the performance results of the considered S-PMC shown in Fig. 1 at rated conditions (slip = 3%). It can be seen that the q-axis current of the fundamental harmonic is the largest of the current components. Furthermore, it can be seen that the peak value of zero-sequence current $I_{o(3)}$ is comparable to that of the 5^{th} harmonic dq-currents.

Also shown in Table II is the $dq0$-axis inductances as calculated from (22). It can be seen that the harmonic self-inductances are of comparable magnitude and that the harmonic mutual-inductances are of negligible magnitude.

The S-PMC torque components of (27) are determined separately for the respective individual harmonic components and are given in Table II. It can be seen that the PM-flux linkage torque of the fundamental component $T_{pm(1)}$ is the main contributor to the developed torque, whereas the zero-sequence and 5^{th} harmonic torque components are negligibly small. Furthermore, the reluctance T_r and cross-magnetization T_m torque components are negligible.

TABLE II
PERFORMANCE PARAMETER VALUES AT RATED CONDITIONS OF PM-SLIP COUPLER.

1^{st} Harmonic		3^{rd} Harmonic		5^{th} Harmonic	
Parameter	Value	Parameter	Value	Parameter	Value
Current	A	Current	A	Current	A
$I_{d(1)}$	137.5	$I_{o(3)}$	-24.38	$I_{d(5)}$	-8.81
$I_{q(1)}$	422.7	——	——	$I_{q(5)}$	-28.6
Inductance	nH	Inductance	nH	Inductance	nH
$L_{d(1)}$	378			$L_{d(5)}$	353.1
$L_{q(1)}$	435	$L_{o(3)}$	389	$L_{q(5)}$	355.7
$M_{dq(1)}$	21			$M_{dq(5)}$	3.4
Torque	Nm	Torque	Nm	Torque	Nm
$T_{pm(1)}$	40.9			$T_{pm(5)}$	0.039
$T_{r(1)}$	-0.34	$T_{o(3)}$	-1.23	$T_{r(5)}$	0
$T_{m(1)}$	0.36			$T_{m(5)}$	0

C. Verification

To validate the results of the proposed S-FE method, the S-PMC of Fig. 1 is also modelled using the commercial transient-FE (T-FE) package *JMAG Designer*.

Fig. 5 shows the coil current versus rotor position at slip = 1% and at rated slip (3%) as determined by the T-FE program *JMAG Designer* and the S-FE solution method. It can be seen that a good agreement between the results is obtained. It is clear that the 3^{rd} harmonic and the 5^{th} harmonic components have a significant effect on the shape of the coil current and that the assumption that the coil currents are sinusoidal isn't valid for this S-PMC topology.

Fig. 6 shows the results for current harmonic amplitude versus slip percentage for the S-FE and T-FE solutions. From this, it can be seen that a good agreement between the results is achieved over a wide slip range, which validates the effectiveness of the proposed S-FE solution method.

Fig. 7 shows the results for the developed torque of the considered S-PMC as determined by the T-FE solution and the proposed S-FE solution method. As can be seen, a very good agreement between the results is achieved over a wide slip range.

VII. Discussion of the Proposed Solution Method

With reference to Fig. 3, the average time taken for the proposed S-FE method to solve the S-PMC currents is approximately 100 seconds. The mesh used in the S-FE method consists of 12030 elements and 7001 nodes. This was done on a Intel(R) core i7 CPU which has a clock speed of 3.40 GHz with 16 GB of RAM. In comparison, on the same computer and with a similar number of mesh elements (12988) and nodes (6928), the commercial T-FE program *JMAG* requires on average approximately 900 seconds to provide a convergent solution for the S-PMC currents. Hence the proposed S-FE method is 9 times faster than the T-FE solution which is a significant reduction in computation time, something which is very important in design optimization applications.

It should be noted the proposed S-FE method presented in this paper considers the 5^{th} harmonic as the highest-order harmonic component present in the coil currents, however, the proposed method is suitable for the prediction of even higher-order harmonics. However, additional harmonics will result in longer simulation times. Furthermore, if certain higher-order harmonic currents are found to be negligible, the number of linear FE-solutions per iteration can be reduced, which will reduce the solution time of the proposed S-FE solution method.

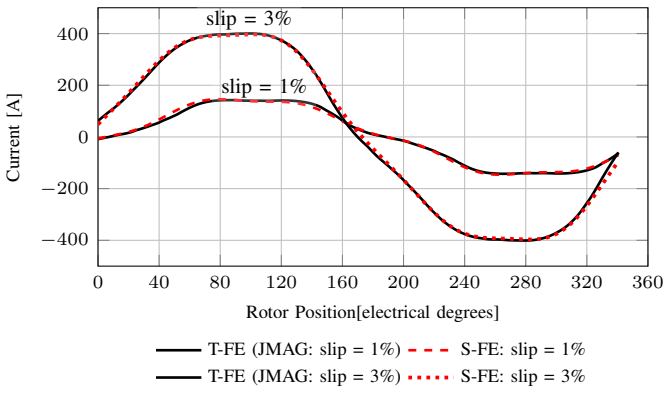

Fig. 5: Transient- and static-FE comparison of coil current versus electrical rotor position for slip = 1% and 3%.

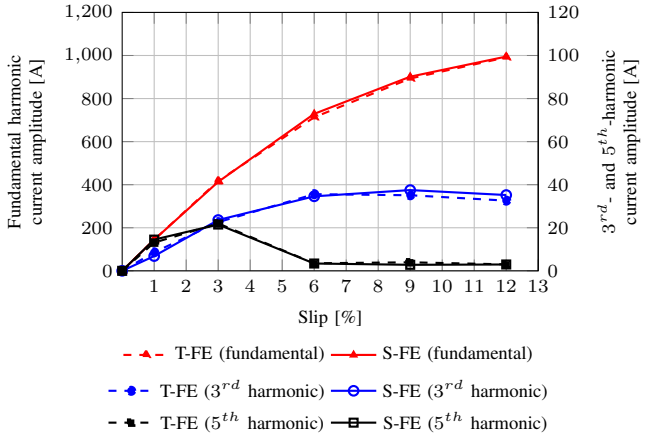

Fig. 6: Transient- and static-FE current harmonic amplitudes versus slip percentage. The fundamental current harmonic amplitude is on the primary y-axis and the 3^{rd} and 5^{th} current harmonic amplitudes are on the secondary y-axis.

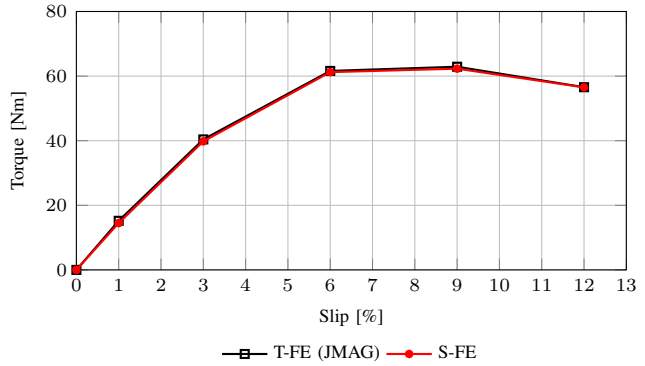

Fig. 7: Torque comparison showing the average torque versus slip as determined by the transient-FE and the proposed static-FE solutions. Rated slip is at 3%.

VIII. Conclusion

A 2-D static-FE modelling and performance solution method for iron-cored PM slip couplers is proposed and evaluated in the paper. Particular attention is given to the zero-sequence (3^{rd} harmonic) and 5^{th} harmonic parameters, and the performance of the coupler. The main findings are summarized as follows.

The proposed solution method is shown to solve the $dq0$ currents of the coupler within four iterations fairly independent of the given slip value. The accuracy of the solution value over a wide slip range is confirmed by transient-FE commercial package solutions. Furthermore, the proposed method is fast and ideally suited for the design optimisation of these PM slip couplers.

It was found that the zero-sequence and 5^{th} harmonic

currents have a significant effect on the shape of the coil current and that the coil currents of PM slip couplers cannot necessarily be considered sinusoidal. Furthermore, it is shown by theory and proved by the proposed S-FE calculation method that the zero-sequence and 5^{th} harmonic induced currents contribute to the torque developed of the slip coupler.

With the zero-sequence circuit at three-times slip frequency and the 5^{th} harmonic circuit at five-times the slip frequency, their respective reactances relative to the coil resistance quickly increases with slip frequency. Hence, the relatively largest effect the zero-sequence and 5^{th} harmonic induced currents have on the performance of the coupler is at low loads.

REFERENCES

[1] T. Yamaguchi, Y. Kawase, H. Kodama, K. Hirata, Y. Hasegawa and T. Ota, "Eddy current damping analysis of laser marker using 3-D finite element method," in IEEE Transactions on Magnetics, vol. 42, no. 4, pp. 1011-1014, April 2006.

[2] H. K. Razavi and M. U. Lamperth, "Eddy-current coupling with slotted conductor disk," in IEEE Transactions on Magnetics, vol. 42, no. 3, pp. 405-410, March 2006.

[3] T. F. Chan, W. Wang and L. L. Lai, "Performance of an Axial-Flux Permanent Magnet Synchronous Generator From 3-D Finite-Element Analysis," in IEEE Transactions on Energy Conversion, vol. 25, no. 3, pp. 669-676, Sept. 2010, doi: 10.1109/TEC.2010.2042057.

[4] S. Orlova, M. Konuhova, E. Kamolins, R. Otankis and A. Suleiko, "Design of Magnetic Couplings for Bioreactors: Analytical Treatment and Optimization," 2018 20th European Conference on Power Electronics and Applications (EPE'18 ECCE Europe), 2018, pp. P.1-P.10.

[5] W. Zhong, Z. Mao, W. Tian and Y. Li, "Design and performance analysis of trapezoid Halbach array magnetic couplings for Ocean current turbine generator," Global Oceans 2020: Singapore – U.S. Gulf Coast, 2020, pp. 1-5, doi: 10.1109/IEEECONF38699.2020.9389141.

[6] E. P. Furlani, "Formulas for the force and torque of axial couplings," in IEEE Transactions on Magnetics, vol. 29, no. 5, pp. 2295-2301, Sept. 1993.

[7] J. -. Charpentier and G. Lemarquand, "Optimal design of cylindrical air-gap synchronous permanent magnet couplings," in IEEE Transactions on Magnetics, vol. 35, no. 2, pp. 1037-1046, March 1999.

[8] R. Ravaud, G. Lemarquand, V. Lemarquand and C. Depollier, "Permanent Magnet Couplings: Field and Torque Three-Dimensional Expressions Based on the Coulombian Model," in IEEE Transactions on Magnetics, vol. 45, no. 4, pp. 1950-1958, April 2009, doi: 10.1109/TMAG.2008.2010623.

[9] Z. Meng, Z. Zhu and Y. Sun, "3-D Analysis for the Torque of Permanent Magnet Coupler," in IEEE Transactions on Magnetics, vol. 51, no. 4, pp. 1-8, April 2015, Art no. 8002008, doi: 10.1109/TMAG.2014.2359851.

[10] J. Wang, H. Lin, S. Fang and Y. Huang, "A General Analytical Model of Permanent Magnet Eddy Current Couplings," in IEEE Transactions on Magnetics, vol. 50, no. 1, pp. 1-9, Jan. 2014, Art no. 8000109.

[11] Y. Chaojun, W. Yingzhi, L. Kang, L. Zhibao, Z. Weifeng and L. Ming, "Analysis for Axial Force of Slotted-Type Axial-Flux Magnetic Coupler," 2017 5th International Conference on Mechanical, Automotive and Materials Engineering (CMAME), Guangzhou, 2017, pp. 359-364, doi: 10.1109/CMAME.2017.8540178.

[12] Y. Li, H. Lin, H. Yang, S. Fang and H. Wang, "Analytical Analysis of a Novel Flux Adjustable Permanent Magnet Eddy-Current Coupling With a Movable Stator Ring," in IEEE Transactions on Magnetics, vol. 54, no. 3, pp. 1-4, March 2018, Art no. 8000404.

[13] J. Wang and J. Zhu, "A Simple Method for Performance Prediction of Permanent Magnet Eddy Current Couplings Using a New Magnetic Equivalent Circuit Model," in IEEE Transactions on Industrial Electronics, vol. 65, no. 3, pp. 2487-2495, March 2018, doi: 10.1109/TIE.2017.2739704.

[14] C. Yang, Z. Peng, J. Tai, L. Zhu, B. J. K. Telezing and P. D. Ombolo, "Torque Characteristics Analysis of Slotted-Type Eddy-Current Couplings Using a New Magnetic Equivalent Circuit Model," in IEEE Transactions on Magnetics, vol. 56, no. 9, pp. 1-8, Sept. 2020, Art no. 8000613, doi: 10.1109/TMAG.2020.3009479.

[15] A. Canova and B. Vusini, "Analytical modeling of rotating eddy-current couplers," in IEEE Transactions on Magnetics, vol. 41, no. 1, pp. 24-35, Jan. 2005.

[16] T. Lubin, S. Mezani and A. Rezzoug, "Simple Analytical Expressions for the Force and Torque of Axial Magnetic Couplings," in IEEE Transactions on Energy Conversion, vol. 27, no. 2, pp. 536-546, June 2012.

[17] S. Hong, J. Choi, S. Jang and K. Jung, "Torque Analysis and Experimental Testing of Axial Flux Permanent Magnet Couplings Using Analytical Field Calculations Based on Two Polar Coordinate Systems," in IEEE Transactions on Magnetics, vol. 50, no. 11, pp. 1-4, Nov. 2014, Art no. 8205304, doi: 10.1109/TMAG.2014.2327954.

[18] B. Dolisy, S. Mezani, T. Lubin and J. Lévêque, "A New Analytical Torque Formula for Axial Field Permanent Magnets Coupling," in IEEE Transactions on Energy Conversion, vol. 30, no. 3, pp. 892-899, Sept. 2015.

[19] T. Lubin and A. Rezzoug, "3-D Analytical Model for Axial-Flux Eddy-Current Couplings and Brakes Under Steady-State Conditions," in IEEE Transactions on Magnetics, vol. 51, no. 10, pp. 1-12, Oct. 2015, Art no. 8203712.

[20] K. Min, J. Choi, J. Kim, H. Cho and S. Jang, "Eddy-Current Loss Analysis of Noncontact Magnetic Device With Permanent Magnets Based on Analytical Field Calculations," in IEEE Transactions on Magnetics, vol. 51, no. 11, pp. 1-4, Nov. 2015, Art no. 8110304, doi: 10.1109/TMAG.2015.2442255.

[21] P. Jin, Y. Tian, Y. Lu, Y. Guo, G. Lei and J. Zhu, "3-D Analytical Magnetic Field Analysis of the Eddy Current Coupling With Halbach Magnets," in IEEE Transactions on Magnetics, vol. 56, no. 1, pp. 1-4, Jan. 2020, Art no. 7501904.

[22] X. Dai, Q. Liang, J. Cao, Y. Long, J. Mo and S. Wang, "Analytical Modeling of Axial-Flux Permanent Magnet Eddy Current Couplings With a Slotted Conductor Topology," in IEEE Transactions on Magnetics, vol. 52, no. 2, pp. 1-15, Feb. 2016, Art no. 8000315.

[23] J. H. J. Potgieter and M. J. Kamper, "Optimum Design and Comparison of Slip Permanent-Magnet Couplings With Wind Energy as Case Study Application," in IEEE Transactions on Industry Applications, vol. 50, no. 5, pp. 3223-3234, Sept.-Oct. 2014.

[24] P. J. J. van Wyk and M. J. Kamper, "Simplified Analysis of Nonoverlap Short-Circuited Coil Winding Slip Permanent Magnet Couplers," in IEEE Transactions on Industry Applications, vol. 52, no. 6, pp. 4740-4751, Nov.-Dec. 2016.

[25] N. Bianchi and S. Bolognani, "Magnetic models of saturated interior permanent magnet motors based on finite element analysis," Conference Record of 1998 IEEE Industry Applications Conference. Thirty-Third IAS Annual Meeting (Cat. No.98CH36242), St. Louis, MO, USA, 1998, pp. 27-34 vol.1.

[26] Gyu-Hong Kang, Jung-Pyo Hong, Gyu-Tak Kim and Jung-Woo Park, "Improved parameter modeling of interior permanent magnet synchronous motor based on finite element analysis," in IEEE Transactions on Magnetics, vol. 36, no. 4, pp. 1867-1870, July 2000.

[27] J. A. Walker, D. G. Dorrell and C. Cossar, "Flux-linkage calculation in permanent-magnet motors using the frozen permeabilities method," in IEEE Transactions on Magnetics, vol. 41, no. 10, pp. 3946-3948, Oct. 2005.

[28] Sang-Yeop Kwak, Jae-Kwang Kim and Hyun-Kyo Jung, "Characteristic analysis of multilayer-buried magnet synchronous motor using fixed permeability method," in IEEE Transactions on Energy Conversion, vol. 20, no. 3, pp. 549-555, Sept. 2005.

[29] M. Mabhula and M. J. Kamper, "Computational Efficient Parameter and Performance Prediction of Wound-Rotor Induction Motor," in IEEE Transactions on Magnetics, vol. 54, no. 6, pp. 1-7, June 2018, Art no. 7401907.

[30] J. H. J. Potgieter and M. J. Kamper, "Calculation Methods and Effects of End-Winding Inductance and Permanent-Magnet End Flux on Performance Prediction of Nonoverlap Winding Permanent-Magnet Machines," in IEEE Transactions on Industry Applications, vol. 50, no. 4, pp. 2458-2466, July-Aug. 2014, doi: 10.1109/TIA.2013.2295468.